DILATOMETRIC STUDIES ON MAGNESIUM AND FLUORINE-CO-SUBSTITUTED HYDROXYAPATITES

Samia NSAR, Ezzedine BEN SALEM, Khaled BOUZOUITA*

U.R. Matériaux Inorganiques, Institut Préparatoire aux Etudes d'Ingénieur de Monastir, 5000 Monastir, University of Monastir, Tunisia

(Reçu le 25 Octobre 2011, accepté le 18 Juin 2012)

ABSTRACT: Magnesium- and fluoride-co-substituted hydroxyapatites ($Ca_9Mg(PO_4)_6(OH)_{2-y}F_y$, where $0 \leq y \leq 2$, have been synthesized by the hydrothermal method. The X-ray diffraction showed that all the powders were single-phased. The sintering behavior of powders was studied by dilatometry from 25 to 1200°C, and the sintered samples were investigated by using the XRD and scanning electron microscopy. During heating, there was a decomposition of the apatite due to the presence of Mg. The nature of the formed products was closely related to the fluorine content. For the compositions rich in fluorine, the end of the shrinkage was interrupted by the formation of a liquid phase thereby inducing the crystallization of needle like-crystals through a dissolution-diffusion-reprecipitation process.

Keywords: Apatite; Sintering; Thermal behavior

RESUME: Des hydroxyapatites co-substituées au magnésium et au fluor ($Ca_9Mg(PO_4)_6(OH)_{2-y}F_y$), où $0 \leq y \leq 2$, ont été synthétisées par la méthode hydrothermale. La diffraction des rayons X a montré que toutes les poudres étaient monophasées. Le comportement au frittage des différents composés a été étudié par dilatométrie de 25 à 1200°C, et les échantillons frittés ont été analysés par DRX et microscopie électronique à balayage. Pendant le chauffage, la décomposition de l'apatite a été reliée à la présence de Mg. La nature des produits formés dépendait étroitement de la teneur en fluor. Pour les compositions riches en fluor, la fin de retrait a été interrompue par la formation d'une phase liquide, induisant la cristallisation des poudres sous forme de bâtonnets, selon un processus de dissolution-diffusion-reprécipitation.

Mots-clés: Apatite; Frittage; Comportement thermique

1. INTRODUCTION

Hydroxyapatite ($Ca_{10}(PO_4)_6(OH)_2$, HA) is the main ceramic material employed in dental, orthopedic and maxillofacial applications thanks to its chemical composition and crystallographic structure similar to those of mineral bones [1], which contribute largely to its bioactivity and biocompatibility [2,3]. However, there is a significant difference between the apatite contained in the mineral bone and the synthetic HA. Biological apatite is nonstoichiometric, poorly crystallized and containing several trace elements like Na^+, Sr^{2+}, Mg^{2+}, F^-, Cl^-, CO_3^{2-}, etc. As these differences play a significant role in the physical, biological and mechanical properties of the apatite, a particular attention has been paid in the last 30 years to the improvement of the hydroxyapatite behavior in the human body.

Thus, several studies have been carried out in order to determine the substitution effect of calcium, phosphorus and hydroxyl group by other species such as those listed above. Among them, magnesium and fluorine are known to play an important role in many biological functions [4-6].

Fluorine is considered a powerful protective-agent against dental caries [7], it strengthens the bone structure [8] and improves the bonds between the bone and implant [9-11]. Furthermore,

* Corresponding author, email : khaled.bouzouita@ipeim.rnu.tn
Tel: +216 20 496 468; Fax: 216 73 500 512

fluorine increases the cristallinity and stability of the apatite and decreases its solubility [12-24]. Therefore, when fluorine is incorporated into bone mineral, its resorption is reduced.

Magnesium is one of the most important minerals in the body [25]. It is needed for more than 300 biochemical reactions. Nevertheless, approximately 50% of the total human body amount is found in the skeleton [26,27]. A magnesium deficiency alters the calcium metabolism [28]. This creates an imbalance in the osteoblast and osteoclast activities leading to bone fragility [29]. The joint administration of Mg and F seems to have a more beneficial effect [30-32]. Unlike the fluorine, the incorporation of Mg into the HA structure inhibits its crystallization, increases its dissolution and affects its thermal stability [13,33-40].

Thus, the literature review reveals that the incorporation of Mg or F into the hydroxyapatite was widely investigated. Also, reports on the co-substituted hydroxyapatite with Mg and other cations or F and other anions are found in the literature [41,42]. Nevertheless, only few articles, recently published, were devoted to the synthesis of Mg/F-co-substituted hydroxyapatites [32,43] or to obtain hydroxyapatite-β-tricalcium phosphate composites with co-substituted elements such as Mg, Na and F [44] or Mg, K, Na F and Cl [45]. However, no studies on the sintering behavior of these materials are available in the literature.

The aim of this work is to investigate the sintering behavior of Mg/F-co-substituted hydroxyapatite powders using dilatometry, XRD and SEM.

2. EXPERIMENTAL PROCEDURE

The Mg-containing hydroxyfluorapatites were prepared via the hydrothermal method, using $Ca(NO_3)_2.4H_2O$, $Mg(NO_3)_2.6H_2O$, $(NH_4)_2HPO_4$ and NH_4F as the starting reagents. Appropriate amounts of these reactants were weighed according to the stoichiometric formula of $Ca_9Mg(PO_4)_6(OH)_{2-y}F_y$, where y = 0.0, 0.5, 1.0, 1.5, and 2, and introduced with 5 cm^3 of deionized water in a Teflon vessel (model 4749 Parr Instrument). The pH of the mixed solution, maintained under vigorous stirring was adjusted to 9 by the addition of a concentrated ammonium hydroxide solution. After that, the sealed autoclave was put into an oven and the temperature was raised to 180ºC, followed by a holding time period of 6 h. Then, the oven was naturally cooled. The precipitates were filtered, washed with deionized water and dried at 70 ℃ for 24 hours.

In the following sections, the samples with y = 0, 0.5, 1, 1.5 and 2 will be labeled as MHA, $MHF_{0.5}A$, MHF_1A, $MHF_{1.5}A$ and MFA, respectively.

The obtained powders were submitted to a chemical analysis. Calcium and magnesium were analyzed by the atomic absorption spectroscopy. Phosphorus was estimated by the phosphovanadomolybdate method [46] and fluoride potentiometrically with a specific ion electrode.

The phase compositions of the as-prepared powders and sintered samples were determined by the X-ray diffraction (XRD) (Philips PW 1800 diffractometer) using Cu-Kα radiation. Scans were run from 20 to 55° with a step size of 0.1, and a counting time of 1 s per step. The lattice parameters of the as-prepared powders and the phase distribution for the sintered samples were determined by the Rietveld refinement of the XRD data using the Fullprof program [47].

The specific surface area (SSA) of the as-prepared powders was measured by the BET method using N_2 as an adsorption gas (Belsorp 28 SP). The primary particle size, D_{BET}, was estimated by assuming the primary particles to be spherical:

$$D_{BET} = \frac{6}{\rho.s} \quad (1)$$

where ρ and s are the theoretical density and the SSA of the powder, respectively.

The particle size of the powders was also analysed by laser granulometry (Malvern instruments, Mastersizer 2000).

The dilatometry was conducted using a Setaram TMA 92 dilatometer on the as-prepared powders. Pellets of 10 mm in diameter and 5 mm in thickness were uniaxially pressed and used as samples. A heating rate of 10℃/min was employed up to 1200℃.

The microstructures of the sintered ceramics were studied using the scanning electron microscopy (PHILIPS SEM, Model XL 30).

3. RESULTS AND DISCUSSION

3.1. Starting powders

The results of the chemical analysis of the as-synthesized powders are summarized in Table I. For all the samples, the (Ca+Mg)/P molar ratios were similar to the theoretical value of 1.67. In addition, as shown in Table I, the fluoride amounts were close to the nominal content.

Table I: Chemical analysis data of as-prepared powders

	Compositions (atoms)				
	MHA	$MHF_{0.5}A$	MHF_1A	$MHF_{1.5}A$	MFA
Ca	9.035	8.860	9.037	9.035	8.880
Mg	0.900	0.940	0.960	0.960	0.916
P	5.900	5.890	5.980	5.960	5.890
F	-	0.510	0.980	1.500	1.920
Ca + Mg/P	1.680	1.663	1.671	1.677	1.663

The XRD patterns of the powders are presented in Fig. 1. All the XRD patterns matched the standard for HA (JCPDS #09-0432) or FA (JCPDS #00-071-0880), and no secondary phases were detected for any of the different compositions. The gradual shift of the position of the peak (300) towards the higher angles as the fluorine content increased is an evidence of the incorporation of F^- into the apatite structure, and the formation of the MHFA solid solution (Fig. 1). It is well known that the substitution of F^- for OH^- induces the contraction of the *a* parameter while *c* remains

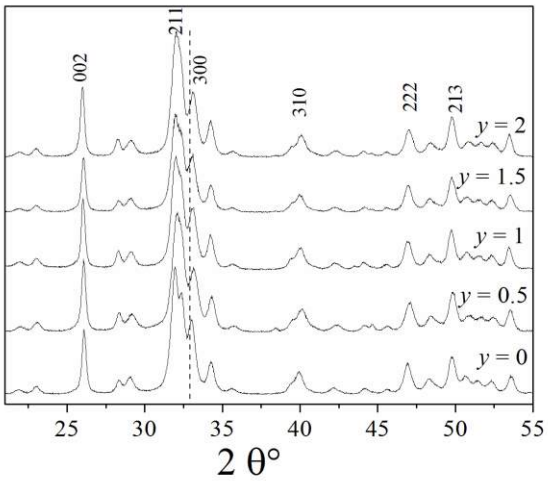

Fig. 1: XRD patterns of as-prepared powders.

practically constant [16]. The insertion of Mg within the HF_1A lattice can be evidenced by comparing the lattice parameters of the MHF_1A sample with those of HF_1A. The calculated values of *a* and *c* are 9.386(2) Å and 6.861(5) Å, and 9.398(4) Å and 6.873(2) Å, respectively. The decrease in the lattice parameters of MHF_1A confirms the incorporation of Mg, in agreement with its size (0.72 Å) smaller than that of Ca^{2+} (1.00 Å).

The particle size and the SSA are some of the most important properties, which are necessary to consider because the sintering as well as the mechanical properties of ceramics strongly depend on these parameters [48]. The characteristics of the as-synthesized powders are illustrated in Table

II. Compared to HFA, the SSA value of MHF_1A is higher, respectively 47 and 59 $m^2.g^{-1}$. This is in line with the inhibitor role of Mg on the apatite crystallization in solution [33-40]. For the Mg-substituted hydroxyfluorapatites, in agreement with the literature for the hydroxyfluorapatites [12,14], the SSA increased as the content of F^- ions did, reached a maximum for x = 0.8-1.0 and then decreased. This maximum in the SSA was related to the interaction between the fluoride and hydroxyl ion. However, in the present case, the maximum was observed for y = 0.5. Assuming the powder particles to be spherical in shape, the average sizes were calculated using Eq. (1) (Table II). The D_{BET} values follow the same variation as the SSA.

Table II: the specific surface area measurements and particle size values (D) of the as-prepared powders

	Compositions				
	MHA	$MHF_{0.5}A$	MHF_1A	$MHF_{1.5}A$	MFA
SSA (m2/g)	49	63.8	59	54	51.7
D_{BET} 10^{-3} (µm)	39	30	32	35	36
D_{50} (µm)	12	9.2	8.4	7.6	4.1

The particle size distribution of the powder was also determined by using the dynamic laser scattering method (Fig. 2). Regarding this figure, it appears that the particle size distribution of the powders was multimodal: the first particle population had a narrow size distribution 0.1-0.4 µm while the particles corresponding to the second population were distributed in a wider size range 1-70 µm. A third population is observed for MHA (80-300 µm). It is interesting to note that for y = 0.5, the particle size distribution had a different shape from those of the other powders. The peak corresponding to the second population is much broader. The size distribution varies from 1 to 400 µm. This change in the particle size distribution may presage a change in the behavior of this composition. The mean particle sizes, D_{50}, of the powders are given in Table II, too. These values are much higher than those of D_{BET}, indicating that the powders were agglomerated. This could be resulting from the agglomeration of particles with the submicrometer sizes (first population) consecutive to the increase of attraction between them with a decreasing particle size due to Van der Waals interaction [49-51].

According to the literature, the incorporation of Mg^{2+} leads to the decrease of the temperature decomposition of the hydroxyapatite [33-40] while with the substitution of F^- for OH^-, the temperature onset of the thermal decomposition increases with the increase of the fluoride content [12-24]. The ATG analysis performed on these powders confirms that Mg and F have an opposite effect on the thermal stability of HA [43]. Compared to the HFA, MHFA decomposed at a much lower temperature. This was related to the presence of Mg, which destabilizes the HA structure [33-40]. For MHF_yA, a shift in the decomposition temperature to higher values was observed when the F content increased, in agreement with the stabilizing role of fluorine [12-24].

3.2. Sintering behavior

Fig. 2 displays the shrinkage behavior and the shrinkage rate of powder compacts versus the temperature. For MFA, as described in the literature [52,53], the shrinkage occurred in two steps (Fig. 2e). The first one started at about 600 °C, and achieved a maximum sintering rate at 670 °C. The second step, corresponding to the major densification, reached a maximum rate at about 940 °C. From 1050 °C, an expansion with a low amplitude was observed. The overall linear shrinkage was found to be 18.7 %. In contrast, for $MHF_{1.5}A$ and MHF_1A, the shrinkage took place practically in one step beginning at about 570 and 650 °C, respectively, and its maximum was located at 855 and 940 °C, respectively. An expansion of the samples occurred at about 1020 and 1125 °C,

respectively. Before the expansion, the shrinkage, which was complete, reached values of 20 and 18.2 %, respectively.

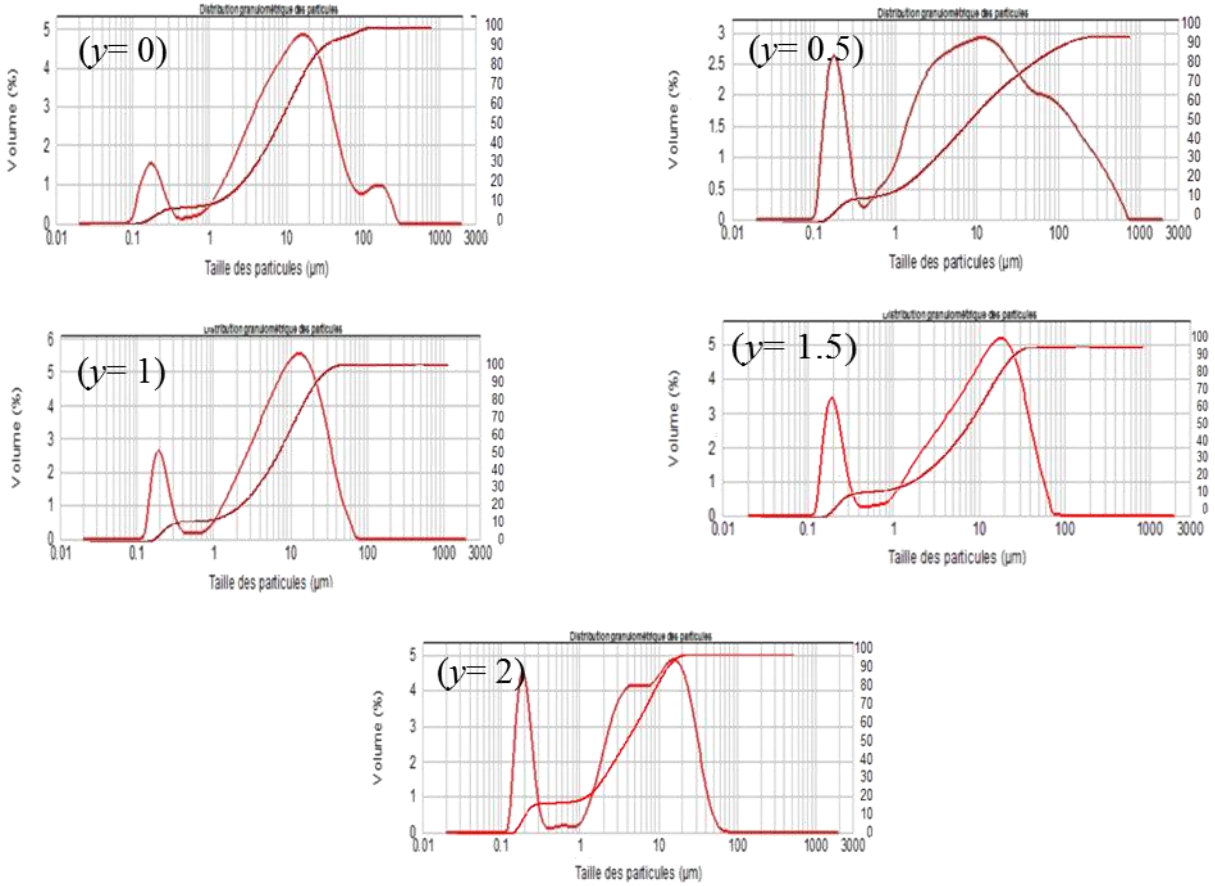

Fig. 2: Particle size distribution of as prepared powders.

As for MFA, the shrinkage for $MHF_{0.5}A$ and MHA occurring in two steps started at 646 and 670 °C, respectively with a maximum for the major densification at 1060 and 1044 °C (Fig. 2b, a). However, for the latter material, the first one was minor whereas it was around 5% for $MHF_{0.5}A$. It is more important than that for MFA. Unlike materials with $y > 0.5$, these two materials did not expand at the end of the densification. The total shrinkage for both materials was approximately 18%.

Compared to MHA, the linear shrinkage of MFA was slightly larger, and the temperature at which the powder began to shrink and that at which the sintering rate was maximum were much lower, indicating a higher sinterability of this material. This behavior cannot be explained only by the SSA of the powder, which was slightly higher (Table II), it would be related to the mobility of F^- species, higher than that of OH^- ones [12, 18]. For $MHF_{0.5}A$, although it had the highest SSA value (Table II), it exhibited the lowest sinterability among all the samples. The SSA is known to be the driving force of the densification. Furthermore, the mobility of the fluoride ions higher than those of the hydroxyl ones should improve the densification. With respect to MHA, the low sinterability of $MHF_{0.5}A$ might be ascribed to the interactions between the hydroxyl and fluoride ions, limiting thus their diffusion [12], and consequently the densification of the material. Gross and co-workers [18] and Senamaud and co-workers [12] studying the sintering of hydroxyfluorapatite had observed that a large decrease in density occurred for the 60% and 50% fluorided samples, respectively. They attributed this decrease in density to the interactions occurring between fluoride and hydroxyl ions. Indeed, when the fluoride ion is present in the hydroxyapatite network, a

hydrogen bond is formed between these ions and the hydroxyl ones [54], which reduces the mobility of these species, and consequently the densification.

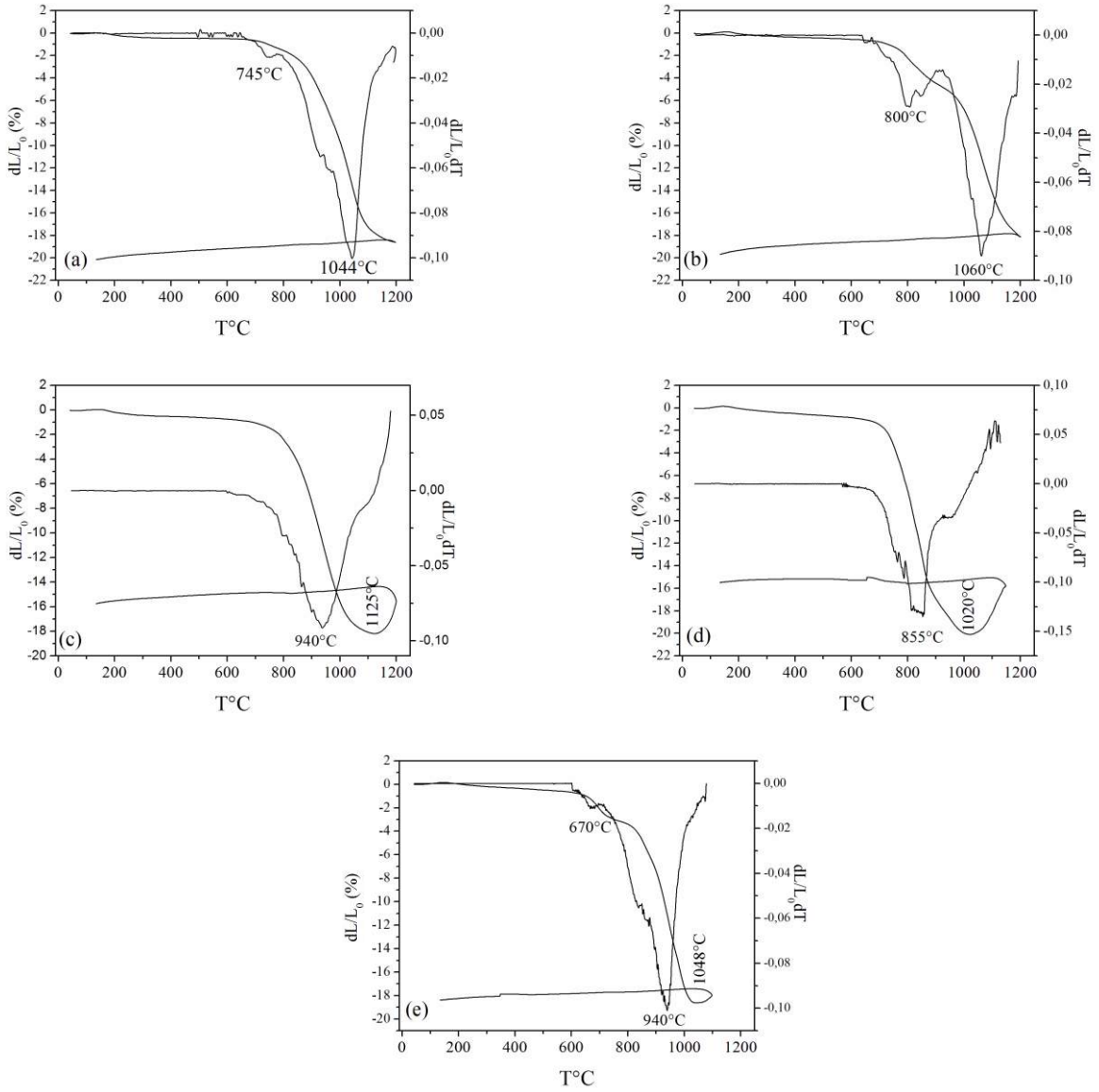

Fig. 2: Shrinkage and shrinkage rate curves of the MHF_yA ($0 \leq y \leq 2$) samples sintered up to 1200°C: (a) MHA, (b) $MHF_{0.5}A$, (c) MHF_1A, (d) $MHF_{1.5}A$ and (e) MFA.

For MHF_1A and $MHF_{1.5}A$, the shrinkage curves should also include two steps as is the case for the other materials. The observation of the shrinkage rate curves, particularly that of MHF_1A, shows that they include many shoulders suggesting that the shrinkage occurred in a succession of steps. We notice that for these materials, the interactions between F^- and OH^- should still exist, and their maximum effect should be observed for the latter sample [12].

Fig. 3 shows the XRD patterns of the samples sintered at 1000 °C for 1 h. For MHA and $MHF_{0.5}A$, besides the apatite, the patterns contained extra peaks indexed for the β-Mg-substituted tricalcium phosphate (β-MTCP) on the basis of JCPDS card #070-0682. It is well known that Mg destabilizes the hydroxyapatite and favors its thermal decomposition into β-MTCP [13,33,35,38]. For MHF_1A, XRD analysis revealed in addition to MTCP the stanfieldite ($Ca_4Mg_5(PO_4)_6$) (JCPDS #11-0231), while for $MHF_{1.5}A$, this latter phase was the only secondary phase detected. In the case

of MFA, the secondary phase was the wagnerite, Mg_2FPO_4 (JCPDS #00-074-1236). Thus, during the sintering, the apatite decomposed. However, at a given temperature, when the F content increased up to y = 1.5, the amount of the secondary phases decreased (Table III), indicating that the structure became more stable. Furthermore, the nature of the decomposition products is in connection with the fluorine content.

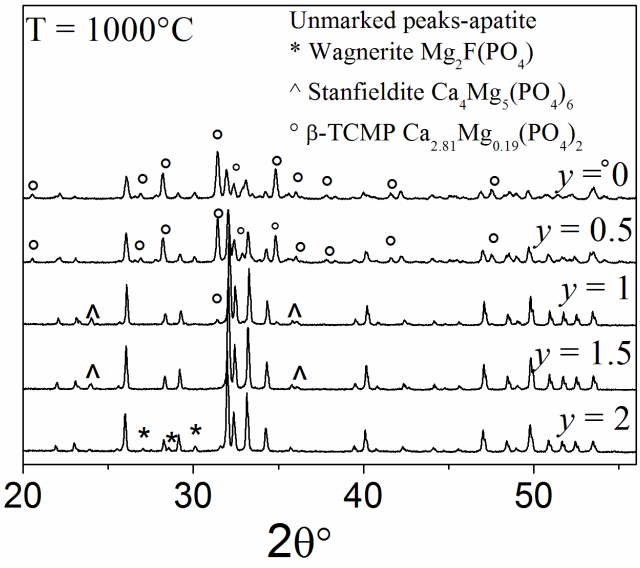

Fig. 3: XRD patterns of sinterd powders at 1000°C for 1 h.

Table III: Phase composition of the samples sintered at 1000°C for 1 h (XRD data)

Samples	MHA	$MHF_{0.5}A$	MHF_1A	$MHF_{1.5}A$	MFA
FA/HA wt%	42.67	52.23	87.06	93.6	90.99
MTCP wt%	57.33	47.77	2.23	-	-
$Ca_4Mg_5(PO_4)_4$ wt%	-	-	10.71	6.35	-
Mg_2FPO_4 wt%	-	-	-	-	9.10

Kannan and co-workers [55] have observed that at high temperature, the hydrtoxyfluorapatite has lost a significant amount of fluorine. The lost amount remained constant whatever the incorporated fluorine content is. Table IV shows that there was also a loss of fluorine during the heat treatment but the amount lost, which was important, was not constant. It was closely related to the amount initially inserted.

Table IV: Chemical analysis of Fluorine of the samples sintered at 1200°C for 1 h

samples	MHA	$MHF_{0.5}A$	MHF_1A	$MHF_{1.5}A$	MFA
F (atom)	-	0.09	0.11	0.33	0.43

SEM micrographs of the fracture surfaces of samples sintered at 1000° and 1250°C are shown in Figs. 4 and 5, respectively. In agreement with the dilatometric curves, Fig. 4 shows that at 1000°C the sample $MHF_{0.5}A$ was less densified than the other samples, although its SSA was larger. As indicated previously, this behavior could be ascribed to the interactions between F^- and OH^- species, which limited their mobility. From Fig. 5, two types of microstructure fully consistent with the shrinkage curves can be distinguished. For the MHF_1A, $MHF_{1.5}A$ and MFA samples, the microstructures suggest that there was a formation of a liquid phase during the heat treatment. As observed, they exhibit many large pores in which there are needle-like crystals (Fig. 5c, d, e). The

liquid phase seems to increase with the increase of the fluorine content. Such a microstructure was observed for the magnesium-substituted fluorapatite sintered with additives [56]. For the $MHF_{0.5}A$ sample, the microstructure appears well densified, only few pores appear at the triple grain boundaries (Fig. 4b). At 1250 ° C, The $MHF_{0.5}A$ sample seems better densified than the other samples. This might be due to the lack of the liquid phase on the one hand, and the influence of the temperature whose effect became much more important than that of the interactions between OH^- and F^- on the other hand.

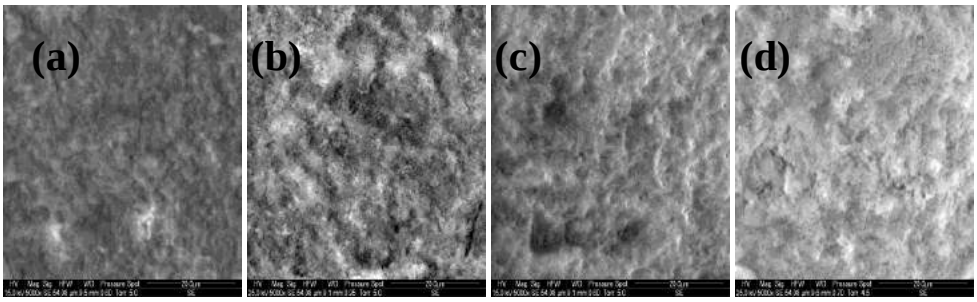

Fig. 4: SEM micrographs of fracture surfaces of the samples sintered at 1000°C for 1h: (a) MHA, (b) $MHF_{0.5}A$, (c) MHF_1A and (d) $MHF_{1.5}A$.

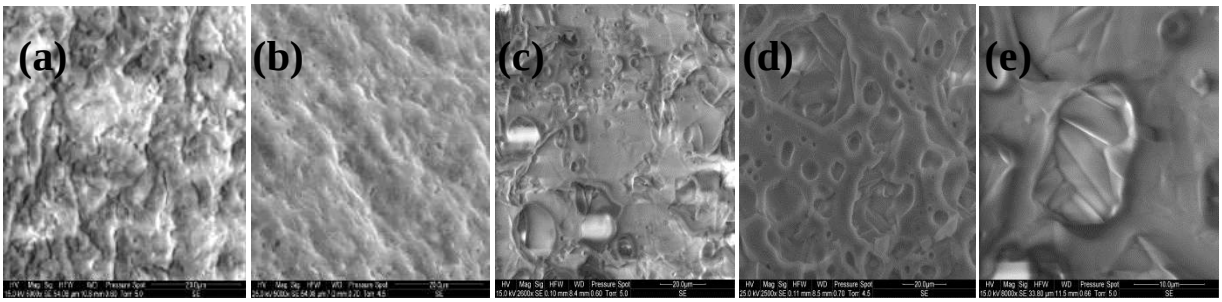

Fig. 5: SEM micrographs of fracture surfaces of the samples sintered at 1250°C for 1h: (a) MHA, (b) $MHF_{0.5}A$, (c) MHF_1A, (d) $MHF_{1.5}A$ and (e) MFA.

A review of the literature revealed that the pure HA [38] and FA [57] as well as the HFA shrink in one step [24]. Therefore, in the present case, the observed shrinkage in two steps would be related to the presence of Mg. Indeed, the dilatometric curves in two steps, obtained by Hidouri [53], and Cacciotti [38] for MFA and MHA, respectively, corroborate this assumption. Also, a sintering behavior in two steps is observed for many other systems. For the sintering of the monazite-brabantite solid solution, the first step is related to the grain coalescence [58] while in the case of the sintering of aluminum nitride in the presence of Y_2O_3, the first step is attributed to the particle rearrangement [59].

In our case, the first step would be attributed to the rearrangement of particles. Indeed, it is well known that the incorporation of Mg into the hydroxyapatite structure inhibits its crystallization in solution and lowers its thermal stability [33,38]. In contrast, the substitution of F^- for OH^- improves the crystallization and the thermal stability of the hydroxyapatite [12,24]. Yet, it seems that the effect of Mg is more pronounced than that of F since all the samples decomposed during the sintering in contrast with the hydroxyfluorapatite solid solutions; the decomposition of the materials could also be responsible for the first stage. Nevertheless, with the increase of the fluorine content, the decomposition product amounts decreased, and the temperature of the onset shrinkage and that

at which the shrinkage was maximum shifted to the low values. This can explain the better densification of the $y = 1.5$ sample.

At the end of the sintering, the observed expansion was due to the formation of a liquid phase resulting from an eutectic between the Mg-substituted hydroxyfluorapatite and impurities present in the starting powders such as CaF_2 [53,60]. This latter was not detected by XRD because, probably, of its low amount. The formation of the liquid phase was also promoted by the presence of Mg.

In the absence of the liquid phase for all the materials, the densification mechanisms during sintering can occur by lattice and/or grain boundary diffusion, while after the formation of the liquid phase, the densification would be governed by the dissolution-diffusion-reprecipitation process leading to the formation of the needle like-crystals.

3. CONCLUSION

Mg-substituted hydroxyfluorapatites powders with the chemical formula $Ca_9Mg(PO_4)_6(OH)_{2-y}F_y$ with $0 \leq y \leq 2$ were prepared using the hydrothermal method. The characterization results can be summarized as follows:

1. The formed solid solution is continuous between the HA and FA limiting phases. No other phosphate compounds were detected in the as-prepared powders.
2. The evolution of SSA with the fluoridation degree is similar to the one reported in the literature for the HFA solid solution. The SSA increased as a function of the fluorine up to $y = 0.5$, and then decreased.
3. The dilatometric study showed that the shrinkage occurred in two stages for MHA, $MHF_{0.5}A$ and MFA, while for MHF_1A and $MHF_{1.5}A$, it took place in one stage. For the compositions rich in fluorine, the shrinkage was interrupted by an expansion, which was attributed to the formation of a liquid phase leading to the crystallization of needle like-crystals according a dissolution-diffusion-reprecipitation process.
4. Among all the samples, $MHF_{0.5}A$ exhibited the lowest sinterability although its SSA was the highest. This is related to the interaction between the fluoride and the hydroxyl ions. However at 1250°C, compared to other samples, it appeared better densified. The effect of the temperature became much more important than that of the interactions between OH^- and F^- ions.
5. During the heat treatment, compared to HA, the Mg lowered the decomposition temperature of MHA while the fluorine increased it. The nature and the amount of the decomposition products were tightly related to the fluorine content inserted in the apatite structure.

REFERENCES

[1] K. S. Katti, *Coll. Surf. B: Biointerfaces*, **2004, 39,** 133.
[2] W. J. A. Dhert, C. P. A. T. Klein, J. A. Jansen, E. A. Van Der Velde, R. C. Vriesde, P. M. Rozing, K. De Groot, *J. Biomed. Mater. Res.*, **1993, 27,** 127.
[3] J. E. G. Hulshoff, K. V. Dijk, J. P. C. M. Van Der Waerden, W. Kalk, J. A. Jansen, *J. Mater. Sci: Mater. Med.*, **1996, 7,** 603.
[4] K. Cheng, W. Weng, H. Wang, S. Zhang, *Biomaterials*, **2005, 26,** 6288.
[5] C. Drouet, M. T. Carayon, C. Combes, C. Rey, *Mater. Sci. Engineering C*, **2008, 28** 1544.
[6] M. Kheradmandfard, M. H. Fathi, M. Ahangarian, E. Mohammadi Zahrani, *Ceram. Intern.* **2012**, **38,** 169.
[7] J.F. McClendon, Wm.C. Foster, N.V. Ludwick, *J. Dent. Res*. **1947, 26,** 233**.**
[8] K.A. Bhadang, C.A. Holding, H. Thissen, K.M. McLean, J.S. Forsythe, D.R. Haynes, *Acta Biomater.* **2010, 6,** 1575.
[9] M. Sundfeldt, M. Widmark, A. Wennerberg, J. Kärrholm, C.B. Johansson, L.V. Carlsson, *J. Mater. Sci.: Mater. Med*. **2002, 13,** 1037.
[10] M. Sundfeldt, J. Persson, J. Swanpalmer, A. Wennerberg, J. Kärrholm, C.B. Johansson, L.V. Carlsson. *J. Mater. Sci.: Mater. Med*. **2002, 13**, 1045.
[11] H. Qu, M. Wei, *Acta Biomater.* **2006, 2,** 113.

[12] N. Senamaud, D. Bemache-Assollant, E. Champion, M. Heughebaert, C. Rey, *Solid State Ionics* **1997, 101-103**, 1357.
[13] E. Bertoni, A. Bigi, G. Cojazzi, M. Gandol, S. Panzavolta, N. Roveri, *J. Inorg. Biochem.* **1998, 72**, 29.
[14] L.M. Rodríguez-Lorenzo, J.N. Hart, K.A. Gross, *Biomaterials* **2003, 24**, 3777.
[15] S.M. Barinov, S.V. Tumanov, I.V. Fadeeva, V.Yu. Bibikov, *Inorganic Mater.* **2003, 39**, 877.
[16] Y. Chen, X. Miao, *Ceram. Inter.* **2004, 30**, 1961.
[17] S.M. Barinov, L.I. Shvorneva, D. Ferro, I.V. Fadeeva, S.V. Tumanov, ***Sci. Tech. Adv. Mater.*** **2004, 5**, 537.
[18] K. A. Gross, L. M. Rodríguez-Lorenzo, *Biomaterials* **2004, 25**, 1375.
[19] K. A. Gross, L. M. Rodríguez-Lorenzo, *Biomaterials* **2004, 25**, 1385.
[20] K. A. Gross, L. M. Rodríguez-Lorenzo, *Biomaterials* **2004, 25**, 1395.
[21] Y. Chen, X. Miao, *Biomaterials* **2005, 26,** 1205.
[22] M.H. Fathi, E.MohammadiZahrani, *J. Crys. Growth* **2009, 311**, 1392.
[23] H. Eslami, M. Solati-Hashjin, M. Tahriri, *Mater. Sci. Engineering* **2009, C29,** 1387.
[24] A. Bianco, I. Cacciotti, M. Lombardi, L. Montanaro, E. Bemporad, M. Sebastiani, *Ceram. Inter.* **2010, 36**, 313.
[25] R.K. Rude, *J. Bone Miner. Res.* **1998, 13**, 749.
[26] P.O. Wester, *Am. J. Clin. Nutr.* **1987, 45**, 1305.
[27] N.E. Saris, E. Mervaala, H. Karppanen, J.A. Khawaja, A. Lewenstam, *Clinica Chimica Acta* **2000, 294,** 1.
[28] M. Elisaf, H. Milionis, K. Siamopoulos, *Mineral Electrolyte Metab.* **1997, 23,** 105.
[29] Institute of Medicine. Food and Nutrition Board. Dietary Reference Intakes: Calcium, Phosphorus, Magnesium, Vitamin D and Fluoride. *National Academy Press*. Washington, DC, **1999**.
[30] R. Sorvari, M. Koskinen-Kainulainen, T. Sorvari, H. Luoma, *Scandinavian J. Dental Research* **1986, 94,** 483.
[31] J. Kur, J. Helbig, G. Anders, K.J. Münzenberg, *Magnesium Bulletin*, **1987**, **9**, 110.
[32] Y. Cai, S. Zhang, X. Zeng, Y. Wang, M. Qian, W. Weng, *Thin Solid Films*, **2009, 517**, 5347.
[33] A. Bigi, G. Falini, E. Foresti, A. Ripamonti, M. Gazzano, N. Roveri, *J. Inorg. Biochem.* **1993, 49,** 69.
[34] S. Ben Abdelkader, I. Khattech, C. Rey, M. Jemal, *Thermochimica Acta* **2001**, **376**, 25.
[35] I. V. Fadeev, L. I. Shvorneva, S. M. Barinov, V. P. Orlovskii, *Inorg. Mater.*, **2003, 9**, 947.
[36] W.L. Suchanek, K. Byrappa, P. Shuk, R.E. Riman, V.F. Janas, K.S. TenHuisen, *Biomaterials* **2004, 25**, 4647.
[37] S. Kannan, I.A.F. Lemos, J.H.G. Rocha, J.M.F. Ferreira, *J. Sol. State. Chem.* **2005, 178**, 3190.
[38] I. Cacciotti, A. Bianco, M. Lombardi, L. Montanaro, *J. Euro. Ceram. Soc.*, **2009, 29**, 2969
[39] F. Ren, Y. Leng, R. Xin, X. Ge, *Acta Biomaterialia*, **2010, 6**, 2787.
[40] D. Laurencin, N. Almora-Barrios, N. H. de Leeuw, C. Gervais, C. Bonhomme, F. Mauri, W. Chrzanowski, J. C. Knowles, R. J. Newport, A. Wong, Z. Gan, M. E. Smith, *Biomaterials*, **2011, 32**, 1826.
[41] S. J. Kalita, H. A. Bhatt, *Mater. Sci. Engineering* **2007, C 27**, 837.
[42] N. Hitmi, C. Lacabanne, R. A. Young, *J. Phys. Chem. Solids* **1988, 49**, 541.
[43] S. Nasr, E. Ben Salem, H. Boughzala, K. Bouzouita, *annl.Chim.* **2011, 36,** 159.
[44] S. Kannan, J. M. F. Ferreira, *Chem. Mater.* **2006, 18**, 198.
[45] S. Kannan, A. F. Lemos, and J. M. F. Ferreira, *Chem. Mater.* **2006, 18,** 2181.
[46] A. Gee, V.R. Deitz, *Ann. Chem. Sci. Mat.*, **1953, 25,** 1320.
[47] J. Rodríguez-Carvajal, *Physica.*, **1993, B192,** 55.
[48] W.D. Kingery, H.K. Borwen, D.R. Uhlmann, 2nd Edition, Introduction to ceramics 2nd edition, J. Wiley editor, **1976**.
[49] H. Ferkel, R. J. Hellmig, *Nanostructured Mater.*, **1999, 11**, 617.
[50] E. Bouyer, F. Gitzhofer, and M. I. Boulos, *J. Mater. Sci.: Mater. Med.*, **2000, 11**, 523.
[51] N. Y. Mostafa, *Mater. Chem. Physics*, **2005, 94**, 333.
[52] S. Nasr, K. Bouzouita, *Bioinorg. Chem. Applications*, **2011**, Article ID 453759, 10 pages doi: 10.1155/2011/453759.
[53] M. Hidouri, K. Bouzouita, F. Kooli, I. Khattech, *Mater. Chem. Phys.*, **2003, 80**, 496.
[54] L.M. Rodriguez-Lorenzo, J.N. Hart, K.A. Gross, *J. Phys. Chem.*, **2003, 107**, 8316.
[55] S. Kannan, J. M. Ventura, and J. M. F. Ferreira, *Chem. Mater.* **2005, 17**, 3065.
[56] M. Hidouri, K. Bouzouita, and N. Fattah, *Annl. Chim. Sci. Mater.*, **2005, 30**,133.
[57] F. Ben Ayed, J. Bouaziz, *C. R. Physique*, **2007, 8,** 101.
[58] B. Glorieux, J.M. Montel, M. Matecki, *J. Eur. Ceram. Soc.*, **2009, 29,** 1679.
[59] M. Tajika, W. Rafaniello, K. Niihara, *Mater. lett.*, **2000, 46,** 98.
[60] E.D.Franz, *Z. Naturforschung*, **1983, 38b,** 1037.